Broadband Piezoelectric Energy Harvesting Induced by Mixed Resonant Modes under Magnetic Plucking

Y. C. Lo, C. C. Chen and Y. C. Shu‡

Institute of Applied Mechanics, National Taiwan University, Taipei 106, Taiwan, R.O.C.

E-mail: yichung@iam.ntu.edu.tw

M. F. Lumentut

School of Civil and Mechanical Engineering and Curtin Institute for Computation, Curtin University, Perth, Australia

E-mail: M.Lumentut@exchange.curtin.edu.au

3 July 2021

Abstract.

A piezoelectric device connected to the standard interface circuit is proposed for harvesting energy by inducing the mixed resonant modes of vibration under the two-point rotary magnetic plucking. It consists of a piezoelectric cantilever beam attached to a tip magnet and a second magnet placed on the middle of the beam. Both magnets are excited by another two magnets aligned radically and attached to a rotating host. The two impulsive forces from these magnets are made in opposite directions for the ease of inducing the second resonant mode. As a result, the harvester device exhibits the pronounced broadband energy harvesting which can not be achieved by the conventional design based on the one-point magnetic plucking for exciting a single resonant mode. The analysis is based on the Fourier decomposition of magnetic impulsive forces for realizing the phenomenon of frequency up-conversion. In addition, the estimate of harvested power is analytically derived based on using the equivalent load impedance which is originally proposed for analyzing harvester arrays. The result shows that the theoretical prediction agrees well with the experimental observation. Further, the rotary frequency response exhibits the remarkable feature of broadband energy harvesting as the output power is increased up to 2500% higher than that in the off-resonance region of the setup allowing plucking only on the tip magnet.

Keywords: Broadband piezoelectric energy harvesting, equivalent load impedance, frequency up-conversion, mixed resonant modes, standard interface circuit, two-point rotary magnetic plucking

‡ Author to whom any correspondence should be addressed.

1. Introduction

Due to escalating demands of the smart sensor device, the electrical energy consumption is essentially required and becomes an increasing visibility in the microsystem technology markets. It is known that the power supply of battery only gives a limited energy source during system operation. As a result, this leads to the time-consuming task for its replacement, which is normally located at the remote area. It then inevitably affects the effectiveness of device usage. To assuage such condition, micro-power harvesting, as a viable alternative engineering solution, can be designed and enables to convert the energy harvesting using a surrounding vibration environment. Such technique has been reported by numerous researchers over the past decade. One of the profound technical capabilities can be found in the use of a smart structure with embedded piezoelectric material. The complete production of the piezoelectric harvesting obviously underlies on the three principles of technical knowledge such as geometry and material properties, fabrications, and power electronic circuits [1, 2].

Nevertheless, the motivation for investigating various models of the piezoelectric vibration-based power harvesting has risen important aspect, particularly for analyzing the electromechanical dynamic system behavior. Starting with the lumped electromechanical parameter models [3], the circuit techniques with various case studies have been developed using the resistive load impedance [4], AC-DC harvesting circuit [5], the synchronized switching harvesting on an inductor (SSHI) [6, 7, 8] and the synchronized electric charge extraction (SECE) [9, 10]. Another work focusing on the continuous vibration modeling with the piezoelectric beam [1, 11, 12, 13, 14] and plate [15, 16, 17] structures has also been developed by considering various mechanical systems and electrical network strategies. Using the multimodal system level of beam arrays, the appearance of multiple resonance peaks can be achieved by using different dimensions of the structures and by tuning further their magnitudes using circuit interface with the SSHI/SECE system [18, 19, 20, 21, 22, 23, 24]. Another alternative way for widening the two-resonance of power output using the nonhomogeneous and discontinuous piezoelectric beam has been investigated using a shunt control [11]. Moreover, tuning the resonances at the higher modes of operations and boosting the optimal power output of the piezoelectric plate structure [16] has been developed using an electrical network of the multiple electrode segments. Finally, the multimodal energy harvesting for broadband improvement can also be achieved by designing specific structures with multiple close peaks of resonances [25]. These include the works of L-shape/meandering beam [26, 27, 28], multi-degree-of-freedom energy harvesters [29, 30, 31, 32], mixed modes of bending and torsion [33, 34], and the harvester beam with a multimodal dynamic magnifier [35].

As clearly seen in the aforementioned literatures, vast majority of the studies for bandwidth improvement, such as array, multimodal and resonance tuning techniques, have been still built on the axial motion excited at around the device's resonances. Therefore, harvesting vibration energy at low excitation frequency is indeed a challenging task for small size of harvesters. A

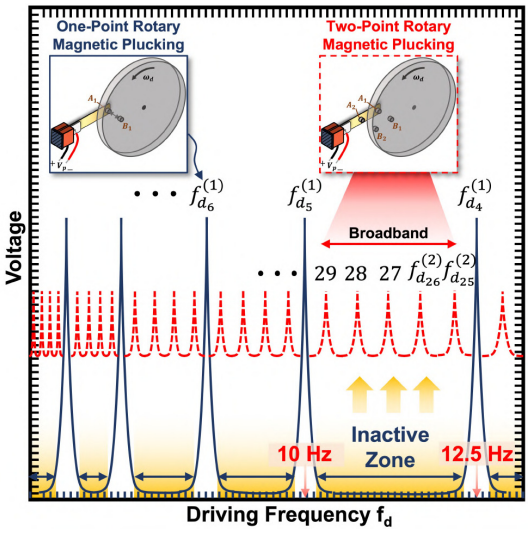

Figure 1. Schematic illustration of introducing the two-point rotary magnetic plucking for broadband frequency up-conversion.

technique for alleviating such condition is to develop frequency up-conversion energy harvesters [36]. This method is to induce a higher-frequency resonance in a transducer from a smaller-frequency motion of ambient source. Therefore, it permits a resonant harvester to operate in a non-resonant practice [37]. Two common strategies for enabling frequency-up include the impact [38, 39, 40] and plucking mechanisms [41, 42, 43]. The former typically implemented by introducing a stopper to limit the amplitude, can broaden bandwidth and harvest more power because of the larger bandwidth [44, 45, 46]. The latter is useful when the energy availability is high and is operated by two different implementations. One is the mechanical plucking transferring energy from the plectrum to the harvester device [47, 48, 49, 50]. The other is the magnetic plucking capable of creating a contactless energy transfer due to a reciprocating excitation [51, 52, 53, 54, 55]. Each of them has its own useful advantages in specific environments, and some of them have shown success in certain applications. For example, the use of magnetic/piezoelectric frequency-up conversion has recently exhibited significant improvements in wrist-worn energy harvesting applied to self-powered smart watches or wristbands [56, 57, 58].

The article is focused on the study of rotary magnetic plucking using the piezoelectric transduction. The conventional design consists of a piezoelectric cantilever beam with a tip magnet. The tip is plucked by another magnet mounted at the lower end of a rotating eccentric disk for human motion powered inertial device [37, 42, 59], or mounted on a rotating plate used for the health monitoring of smart bearings [60]. The setup is based on the one-point rotary magnetic plucking for inducing a single resonant mode of vibration for energy harvesting [51, 61, 62, 63, 64], as illustrated in the upper left corner of Fig. 1. Its operation principle for frequency up-conversion can be described simply by considering a set of discrete driving

frequencies of the plucking force

$$\mathcal{A}_1 = \left\{ f_{d_{n_1}}^{(1)} \;\middle|\; f_{d_{n_1}}^{(1)} = \frac{f_{r_1}}{n_1} \text{ for integer } n_1 \right\}, \tag{1}$$

where f_{r_1} is the first resonant frequency of the harvester beam. It can be shown that the resonance amplification is achieved whenever the driving frequency $f_d \in \mathcal{A}_1$ [51]. But it raises a question about the insufficient voltage output in the inactive frequency zone within the neighboring of peak voltage frequencies. For an example of $f_{r_1} = 50$ Hz, the resonant vibration could be achieved at around $f_{d_4}^{(1)} = 12.5$ Hz ($n_1 = 4$) and $f_{d_5}^{(1)} = 10$ Hz ($n_1 = 5$), as illustrated in Fig. 1. But the voltage frequency response exhibits vanishing output voltage between the adjacent frequencies of 10-12.5 Hz, as also shown in the inactive zone of Fig. 1. This leads to an innovative idea of inducing higher resonant modes for complete broadband energy harvesting. Indeed, consider another set

$$\mathcal{A}_2 = \left\{ f_{d_{n_2}}^{(2)} \;\middle|\; f_{d_{n_2}}^{(2)} = \frac{f_{r_2}}{n_2} \text{ for integer } n_2 \right\}, \tag{2}$$

where f_{r_2} is the second resonant frequency of the harvester beam. Clearly, the set $\mathcal{A}_2$ contains much denser distribution of driving frequencies than the set $\mathcal{A}_1$ due to the wide separation of resonant mode frequencies of the beam. To see it, consider an example of $f_{r_2} = 300$ Hz. The voltage output is sufficiently generated within the frequency range between 10 Hz to 12.5 Hz due to triggering the resonant vibration of the second mode at around the frequencies $f_{d_{n_2}}^{(2)} = 10.3$ Hz, 10.7 Hz, 11.1 Hz, 11.5 Hz and 12.0 Hz for $n_2 = 29, 28, \cdots, 25$, as demonstrated by the red color curves in Fig. 1. It is therefore left to a critical question about how the second resonant mode is induced under plucking with sufficient voltage (power) output. To answer it, a device is proposed and shown to be capable of realizing broadband harvesting energy by inducing the first and second beam resonant modes of vibration. It is achieved by implementing the two-point rotary magnetic plucking, as demonstrated in the upper right corner of Fig. 1. Specifically, it allows two impulsive magnetic forces of opposite directions acting simultaneously on the beam, giving rise to the bending shape similar to that of the second resonant mode. The detailed setup and modeling are described in Section 2. The experiment for validation is described in Section 3 with discussions in Section 4. Finally, the conclusions are made in Section 5.

2. Model

Consider a piezoelectric cantilever beam fixed on the stationary base. Two magnets A_1 and A_2 are attached to the beam and are interacted with the other two magnets B_1 and B_2 placed along the radial direction of the circular rotating plate, as shown in Fig. 2(a). Let L_{r_1} and L_{r_2} be the revolution radii of the magnets B_1 and B_2, and Z_{r_1} and Z_{r_2} be the perpendicular distances between the magnets A_1 & B_1 and A_2 & B_2, respectively, as also shown in Fig. 2(a). Based on the model of dipole-dipole interaction, it can be shown that the magnetic forces acting

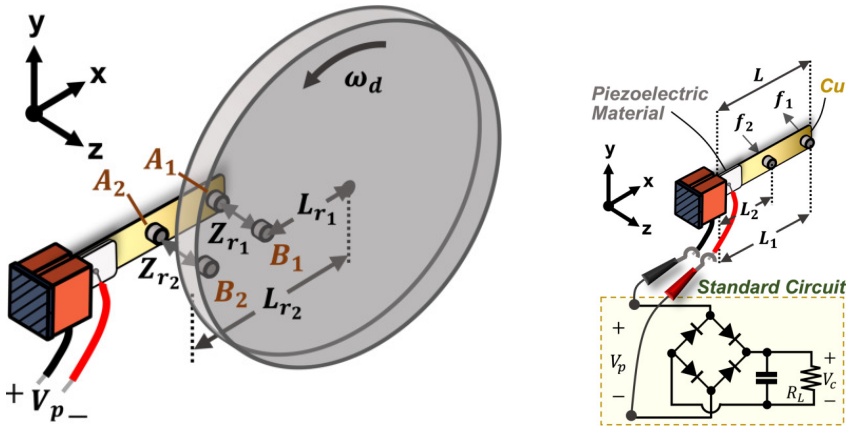

(a) (b)

Figure 2. (a). Schematic presentation of a piezoelectric energy harvester beam impulsively excited by two-point rotatory magnetic plucking. (b). The harvester is attached to the standard interface for AC-DC conversion.

on the magnets A_1 and A_2 are [51]

$$\begin{aligned} f_1(t) &= a_{m_1} \frac{Z_{r_1}\left(Z_{r_1}^2 - \frac{3}{2}d_1^2\right)}{\left(Z_{r_1}^2 + d_1^2\right)^{\frac{7}{2}}}, \quad d_1^2 = 2\left[1 - \cos(w_d t)\right] L_{r_1}^2, \\ f_2(t) &= a_{m_2} \frac{Z_{r_2}\left(Z_{r_2}^2 - \frac{3}{2}d_2^2\right)}{\left(Z_{r_2}^2 + d_2^2\right)^{\frac{7}{2}}}, \quad d_2^2 = 2\left[1 - \cos(w_d t)\right] L_{r_2}^2, \end{aligned} \tag{3}$$

where $w_d = 2\pi f_d$ is the angular driving frequency of the rotating plate and a_{m_i} are the coefficients which can be measured experimentally. Thus, the impulsive force $f(x,t)$ acting on the beam can be expressed as

$$f(x,t) = f_1(t)\delta(x - L_1) + f_2(t)\delta(x - L_2), \tag{4}$$

where $\delta(x)$ is the Dirac delta function, L_1 and L_2 are the positions of the magnets A_1 and A_2 measured from the fixed end of the beam as shown in Fig. 2(b).

Notice that the magnetic forces $f_1(t)$ and $f_2(t)$ are impulsive in nature. Indeed, set

$$\alpha_i = \frac{Z_{r_i}}{L_{r_i}}, \quad \gamma = w_d t, \tag{5}$$

where γ is the angle of revolution. As $f_i(t)$ actually depends on $w_d t$, it can be shown that [51]

$$f_i(\gamma) = \frac{a_{m_i}}{L_{r_i}^4} \frac{\alpha_i \left\{\alpha_i^2 - 3(1 - \cos\gamma)\right\}}{\left\{\alpha_i^2 + 2(1 - \cos\gamma)\right\}^{\frac{7}{2}}} \propto \frac{1}{\alpha_i^4} \tag{6}$$

for small γ. Thus, the peak magnitude of $f_i(\gamma)$ is concentrated at around $\gamma = 0$ and is very sharp for small α_i, as illustrated in Fig. 3(a). Note that the parameters of Fig. 3(a) are drawn from the our experiment shown in Fig. 3(b) which will be described in Section 3.

Next, suppose the harvester is attached to the AC-DC standard interface circuit consisting of a full-bridge rectifier followed by a smoothing capacitor in parallel with a resistive load R_L,

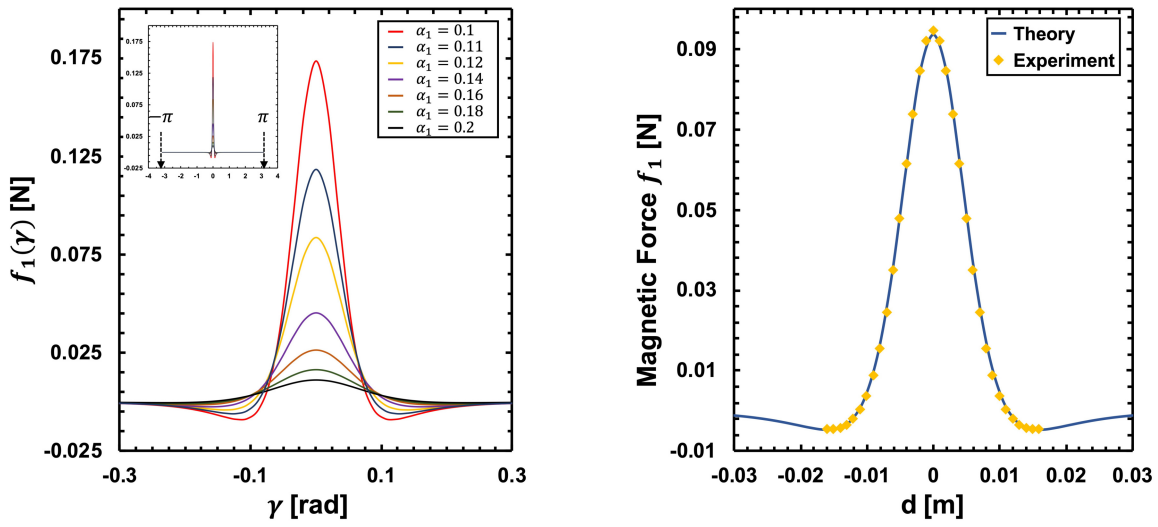

(a) (b)

Figure 3. (a). Illustration of the magnetic force $f_1(\gamma)$ against the angle of revolution γ for various magnitudes of $\alpha_1 = \frac{Z_{r1}}{L_{r_1}}$. (b) The magnetic coefficient a_{m_1} is experimentally determined by fitting the experimental observations (yellow points) to Eq. (3) plotted against the horizontal distance d between two magnets.

as illustrated in Fig. 2(b). The cantilever beam consists of a substrate and a piezoelectric layer partially paved on the top of the beam as also shown in Fig. 2(b). It is excited due to the non-contact rotary magnetic plucking, giving rise to energy harvesting by the direct piezoelectric effect. The explanation is developed according to two different scenarios as presented below.

2.1. Single Resonant Mode Induced by One-Point Rotary Magnetic Plucking

Consider the first case where only the tip magnet A_1 is retained and the second magnet A_2 is removed. This setup is based on the one-point rotary magnetic plucking and has been theoretically studied by Shu et al [51]. We briefly describe their approach below for the ease of extension to the setup of two-point magnetic plucking as shown in Fig. 2. They suggested applying the Fourier technique to the impulsive function $f_1(t)$ for analyzing the phenomenon of frequency up-conversion. Indeed, let

$$f_1(t) = \sum_{n_1} f_{n_1} \cos(n_1 w_d t), \quad f_{n_1} = \frac{2}{\pi/w_d} \int_0^{\frac{\pi}{w_d}} f_1(t) \cos(n_1 w_d t) dt = \frac{2}{\pi} \int_0^{\pi} f_1(\gamma) \cos(n_1 \gamma) d\gamma, \quad (7)$$

where f_{n_1} are the coefficients of the Fourier cosine expansion of $f_1(t)$ defined by Eq. (3). Eq. (7) suggests the resonant vibration of the harvester beam could be achieved as long as $n_1 w_d \approx w_{r_1} = 2\pi f_{r_1}$ where f_{r_1} introduced in Eq. (1) is the first resonant frequency of the beam. Thus, many more discrete peaks appear in the relevant frequency response diagram whenever the driving frequencies are equal to the first resonant frequency divided by some integer, as

indicated by Eq. (1). The device therefore exhibits the phenomenon of the nth frequency up-conversion transforming the low rotational driving frequency into the high resonant vibration.

In addition, it was shown that the electromechanical response of the device could be described by the reduced formulation whenever $n_1 w_d \approx w_{r_1}$ [51]

$$\begin{aligned} M_1\ddot{u_1}(t) + \eta_1\dot{u}(t) + K_1 u_1(t) + \Theta_1 V_p(t) = f_{n_1}\cos(n_1 w_d t), \\ -\Theta_1 \dot{u_1}(t) + C_p\dot{V}_p(t) = -I(t), \end{aligned} \tag{8}$$

where $u_1(t)$ can be viewed as time-varying magnitude of the modal shape function of the first resonant mode, $V_p(t)$ is the voltage across the piezoelectric element, $I(t)$ is the current flowing into the standard interface circuit. Besides, M_1, η_1, K_1, Θ_1 and C_p are the the effective mass, mechanical damping coefficient, the stiffness, the piezoelectric coefficient and the capacitance of the piezoelectric harvester beam. Now we can imitate the familiar case of a harvester under rectilinear harmonic excitation to solve the simplified formulations as in Eq. (8). Indeed, the DC harvested power P_h can be obtained from the work by Shu & Lien (see Eq. (30) in [5]) who analyzed AC-DC power harvesting and showed

$$P_h = \frac{(n_1 w_d)^2 \Theta_1^2 R_L}{\left[\frac{\pi}{2} + (n_1 w_d) C_p R_L\right]^2} \frac{f_{n_1}^2}{\left\{\left[(n_1 w_d)\eta_1 + \frac{2(n_1 w_d)\Theta_1^2 R_L}{\left[(n_1 w_d) C_p R_L + \frac{\pi}{2}\right]^2}\right]^2 + \left[K_1 - (n_1 w_d)^2 M_1 + \frac{(n_1 w_d)\Theta_1^2 R_L}{\left[(n_1 w_d) C_p R + \frac{\pi}{2}\right]}\right]^2\right\}}. \tag{9}$$

2.2. Mixed Resonant Modes Induced by Two-Point Rotary Magnetic Plucking

The conventional magnetic plucking for piezoelectric-based frequency up-conversion harvesters in aforementioned literatures is based on the plucking at the beam tip [51, 53, 61, 62, 64]. This method is, however, not sufficient to excite the higher resonant modes for broadband energy harvesting. It therefore motivates the idea of the inclusion of the second magnetic pair A_2 & B_2 for inducing the resonant vibration of the second mode, as suggested by Fig. 2. The methodology is similar to the previous case based on the one-point magnetic plucking. But there are two main differences. First, the impulsive-like magnetic force $f_i(t)$ will be replaced by the modal forces $F_{r_i}(t)$ which are the linear combination of $f_i(t)$ weighted by the standard modal shape function. Second, the reduced single mode formulations by Eq. (8) will be replaced by the multi-mode coupled formulations whose equivalent circuit model is similar to the case of parallel connection of piezoelectric oscillators excited at different harmonics. The analysis therefore can follow that originally applied to the piezoelectric harvester array connected to different nonlinear interface circuits [18, 19, 20].

Specifically, let the second magnet A_2 be placed at around the middle position of the beam. In addition, the impulsive magnetic forces $f_1(t)$ and $f_2(t)$ are designed to be in the opposite direction. This gives the opportunity for inducing the beam deflection similar to that of the second resonant mode. The deflection of a beam $v(x,t)$ is then approximated to be

$$v(x,t) = u_1(t)\phi_1(x) + u_2(t)\phi_2(x), \tag{10}$$

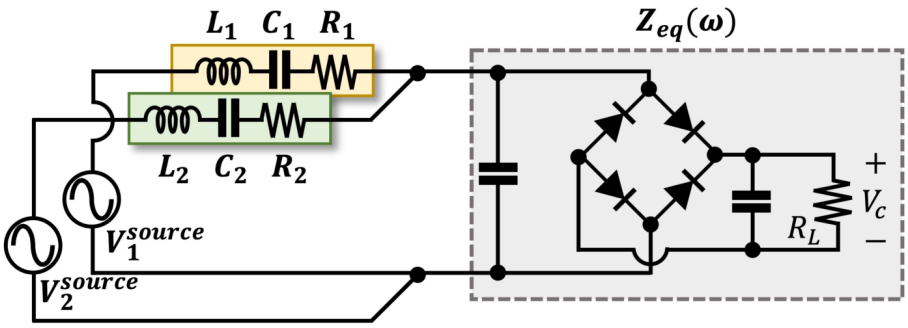

Figure 4. An equivalent circuit model representing two resonant modes of vibration.

where $\phi_1(x)$ and $\phi_2(x)$ are the shape functions of the first and second resonant modes with $u_1(t)$ and $u_2(t)$ as time-varying amplitudes. In the present case of a piezoelectric sheet not covering the whole substrate beam, the determination of these two modal shape functions can be found in literature [65, 66]. In addition, based on the standard modal analysis or the parametric distributed method in piezoelectric harvesters [1], the modal forces $F_{r_1}(t)$ and $F_{r_2}(t)$ on the first and second resonant modes are realized as

$$F_{r_1}(t) = \int_0^L f(x,t)\phi_1(x)dx = \phi_1(L_1)f_1(t) + \phi_1(L_2)f_2(t), \tag{11}$$

$$F_{r_2}(t) = \int_0^L f(x,t)\phi_2(x)dx = \phi_2(L_1)f_1(t) + \phi_2(L_2)f_2(t), \tag{12}$$

where $f(x,t)$ is given by Eq. (4).

To see how the impulsive-like modal force $F_{r_i}(t)$ incites the ith resonant mode of vibration, the Fourier technique briefly described in Section 2.1 is employed again for analyzing the phenomenon of frequency up-conversion [51]. Specifically, the Fourier cosine expansion originally applied to $f_1(t)$ in Eq. (7) is applied to the modal forces $F_{r_i}(t)$ respectively by

$$F_{r_i}(t) = \sum_{n_i} F_{n_i} \cos(n_i w_d t), \quad F_{n_i} = \frac{2}{\pi}\int_0^\pi F_{r_i}(\gamma)\cos(n_i\gamma)d\gamma. \tag{13}$$

It has been shown that F_{n_i} will remain non-vanishing for sufficiently large numbers of n_i if the ratio α_i defined by Eq. (5) is small [51]. Next, if some integers n_1 and n_2 are such that $n_1 w_d \approx w_{r_1}$ and $n_2 w_d \approx w_{r_2}$ ($w_{r_1} = 2\pi f_{r_1}, w_{r_2} = 2\pi f_{r_2}$), the first two resonant modes could be excited simultaneously. The associated reduced formulations are therefore [17, 18]

$$M_1\ddot{u}_1(t) + \eta_1\dot{u}_1(t) + K_1u_1(t) + \Theta_1V_p(t) = F_{n_1}\cos(n_1w_dt), \tag{14}$$

$$M_2\ddot{u}_2(t) + \eta_2\dot{u}_2(t) + K_2u_2(t) + \Theta_2V_p(t) = F_{n_2}\cos(n_2w_dt), \tag{15}$$

$$-[\Theta_1\dot{u}_1(t) + \Theta_2\dot{u}_2(t)] + C_p\dot{V}_p(t) = -I(t). \tag{16}$$

Above, the variables $V_p(t)$, $I(t)$ and the parameters M_i, η_i, K_i, Θ_i and C_p are the same as those defined in Eq. (8). For example K_i is the effective stiffness evaluated at the ith resonant mode.

As the chosen AC-DC interface circuit, shown in Fig. 2(b), consists of nonlinear circuit elements, it makes analyzing Eq. (14) - Eq. (16) much more difficult than the case of simply

attaching to a resistive load. Fortunately, Lien & Shu [18] have introduced the equivalent load impedance $Z_{\rm eq}$ for analyzing the harvester array attached to various nonlinear interface circuits. Based on this approach, it is shown that the circuit elements consisting of the piezoelectric capacitance C_p in parallel with the interface circuit are replaced by an equivalent load impedance $Z_{\rm eq}$, as illustrated by the dashed rectangle box in Fig. 2.2. In the present case of the standard AC-DC interface, $Z_{\rm eq}$ is explicitly expressed by [18]

$$Z_{\rm eq}(w) = \frac{2R_L}{\left(\frac{\pi}{2} + C_p R_L w\right)^2} - j\frac{R_L}{\left(\frac{\pi}{2} + C_p R_L w\right)}, \quad j^2 = -1. \tag{17}$$

Next, Eq. (14) - Eq. (16) can be interpreted by introducing an equivalent RLC circuit model

$$R_i = \frac{\eta_i}{\Theta_i^2}, \quad L_i = \frac{M_i}{\Theta_i^2}, \quad C_i = \frac{\Theta_i^2}{K_i}, \quad V_i^{\rm source}(t) = \frac{F_{n_i}}{\Theta_i}\, e^{jn_i w_d t} \tag{18}$$

as resistor, inductance, capacitance and voltage source, respectively [18]. The piezoelectric voltage V_p related to $Z_{\rm eq}$ gives

$$V_p = (I_1 + I_2) Z_{\rm eq}, \quad I_i(t) = \Theta_i \dot{u}_i(t), \tag{19}$$

where $I_i(t)$ is called the velocity current [18]. This circuit model is schematically presented by Fig. 2.2 and its mathematical formulations in the frequency domain is provided by

$$\bar{V}_1^{\rm source} = \bar{I}_1 \left(jwL_1 + R_1 + \frac{1}{jwC_1} \right) + \left(\bar{I}_1 + \bar{I}_2 \right) Z_{\rm eq}, \tag{20}$$

$$\bar{V}_2^{\rm source} = \bar{I}_2 \left(jwL_2 + R_2 + \frac{1}{jwC_2} \right) + \left(\bar{I}_1 + \bar{I}_2 \right) Z_{\rm eq}, \tag{21}$$

where $\bar{I}_i$ and $\bar{V}_i^{\rm source}$ are the corresponding Fourier transforms of $I_i(t)$ and $V_i^{\rm source}(t)$. It therefore gives

$$\bar{\mathbf{I}} = \mathbf{G}\bar{\mathbf{V}}^{\rm source}, \quad \bar{\mathbf{I}} = \left\{ \begin{array}{c} \bar{I}_1 \\ \bar{I}_2 \end{array} \right\}, \quad \bar{\mathbf{V}}^{\rm source} = \left\{ \begin{array}{c} \bar{V}_1^{\rm source} \\ \bar{V}_2^{\rm source} \end{array} \right\}, \tag{22}$$

where

$$\mathbf{G}(w) = \left[\begin{array}{cc} jwL_1 + R_1 + \frac{1}{jwC_1} + Z_{\rm eq} & Z_{\rm eq} \\ Z_{\rm eq} & jwL_2 + R_2 + \frac{1}{jwC_2} + Z_{\rm eq} \end{array} \right]^{-1}. \tag{23}$$

The harvested power P_h is taken the real part of

$$\frac{1}{2T} \int_0^T \left[I^{\rm tot}(t) \right]^* V_p(t) dt, \tag{24}$$

where $I^{\rm tot} = I_1(t) + I_2(t)$ is the total velocity current, the superscript * denotes the complex conjugate, and T is the period covering $\frac{2\pi}{n_1 w_d}$ and $\frac{2\pi}{n_2 w_d}$. It can be shown that

$$\begin{aligned} P_h = & \frac{F_{n_1}^2}{2\Theta_1^2} \left| G_{11}(w) + G_{21}(w) \right|^2 {\rm Re}\left[Z_{\rm eq}(w) \right] |_{w=n_1 w_d} \\ & + \frac{F_{n_2}^2}{2\Theta_2^2} \left| G_{12}(w) + G_{22}(w) \right|^2 {\rm Re}\left[Z_{\rm eq}(w) \right] |_{w=n_2 w_d}, \end{aligned} \tag{25}$$

where $G_{ij}(w)$ is the ij component of $\mathbf{G}(w)$ defined by Eq. (23).

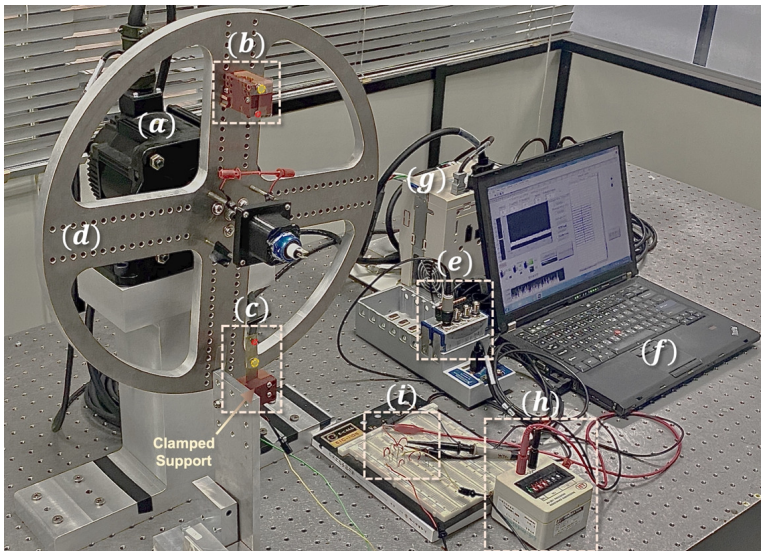

Figure 5. Experimental setup: (a) motor, (b) rotating magnets B_1 and B_2, (c) a piezoelectric cantilever beam with magnets A_1 and A_2 attached on it which is clamped by a fixture, (d) a rotating plate, (e) DAQ for data acquisition, (f) laptop installed with LabVIEW, (g) motor controller, (h) resistance substitution box, (i) standard interface circuit.

Finally, if the resonant frequencies are widely separated as often seen in the beam structure, i.e., $w_{r_1} << w_{r_2}$, then the contributions to power from the crossing terms $G_{12} = G_{21}$ in Eq. (23) are negligible. The harvested power is therefore simplified to be

$$P_h = \sum_i \frac{(n_i w_d)^2 \Theta_i^2 R_L}{\left[\frac{\pi}{2} + (n_i w_d) C_p R_L\right]^2} \times \frac{F_{n_i}^2}{\left\{\left[(n_i w_d)\eta_i + \frac{2(n_i w_d)\Theta_i^2 R_L}{\left[(n_i w_d) C_p R_L + \frac{\pi}{2}\right]^2}\right]^2 + \left[K_i - (n_i w_d)^2 M_i + \frac{(n_i w_d)\Theta_i^2 R_L}{\left[(n_i w_d) C_p R_L + \frac{\pi}{2}\right]}\right]^2\right\}}. \quad (26)$$

3. Experiment

The experimental setup similar to that schematically presented in Fig. 2(a) is now shown in Fig. 5. A cantilever beam is clamped by a fixture mounted on a stationary base. It consists of a Cu substrate and a partial piezoelectric layer made by Eleceram Technology (Taiwan). The size of the Cu substrate is $52.3 \times 15 \times 0.3$ mm^3, and that of the piezoelectric attachment is $7.3 \times 15 \times 0.2$ mm^3. A motor (SGM7G-13AFA61) and its controller (SGD7S-120A00A008) are chosen to drive the rotating plate. The standard interface circuit schematically described by Fig. 2(b) is attached to the harvester. The piezoelectric voltage V_p and the output DC voltage V_c across the load are measured by the designed LabVIEW program for different driving rotational

n_1	3	4	5	6	7	8	9	10	11	12
$F_{n_1}(\times 10^{-3})$	3.355	3.40	3.448	3.50	3.552	3.601	3.646	3.685	3.716	3.739
n_2	16	17	18	19	20	21	22	23	24	25
$F_{n_2}(\times 10^{-2})$	2.169	2.173	2.174	2.173	2.170	2.160	2.150	2.137	2.121	2.102

Table 1. Fourier cosine coefficients F_{n_i} of the magnetic modal forces $F_{r_i}(t)$.

M (kg)	η (N·sec/m)	K (N/m)	Θ (N/V)	C_p (nF)	f^{sc} (Hz)
1.15×10^{-3}	1.45×10^{-3}	114.4	0.936×10^{-4}	12.8	50.2

Table 2. Equivalent parameters of the device under the one-point rotary magnetic plucking. The notation f^{sc} denotes the short-circuit resonant frequency.

frequencies. All of the measurements are recorded through the DAQ device (NI 9229).

There are two magnets A_1 and A_2 attached on the beam and the distances to the end of the beam are $L_1 = 48.0$ mm and $L_2 = 23.0$ mm. Another pair of magnets B_1 and B_2 are aligned radially on the rotating plate with the radii of revolution $L_{r_1} = 117.5$ mm and $L_{r_2} = 142.5$ mm. The perpendicular distance Z_{r_1}between A_1 and B_1 is 10.2 mm and Z_{r_2} between A_2 and B_2 is 9.6 mm. All of these notations are schematically illustrated in Fig. 2.

The measurements start from realizing the magnetic interaction forces characterized by the coefficient a_{m_1} and a_{m_2} in Eq. (3). These two coefficients are obtained by matching the theoretical prediction, as in Eq. (3), to the experimental observations (see, for example, Fig. 5 in [51]). It is illustrated in Fig. 3(b) where the magnetic forces are measured under various horizontal distances d between two magnets. The measured results are $a_{m_1} = 3.3 \times 10^{-9}$ N m^4 and $a_{m_2} = -7.0 \times 10^{-9}$ N m^4. The negative sign in a_{m_2} is due to the opposite directions of magnetic forces $f_1(t)$ and $f_2(t)$. The Fourier coefficients F_{n_1} and F_{n_2} of different modes are therefore determined by numerical integration of Eq. (13) for different integers. The results are listed in Table 1. Next, the equivalent parameters measured at the first resonant mode, as in Eq. (8) for the setup of one-point magnetic plucking, are identified based on the standard modal testing. They are presented by Table 2. Furthermore, for the setup under the two-point magnetic plucking, the equivalent parameters of the harvester beam evaluated at the first and second resonant modes, as in Eq. (14)-Eq. (16), are measured and listed in Table 3.

4. Results and Discussions

The experimental results are discussed according to two different scenarios. Consider the first setup excited by the one-point rotary magnetic plucking. Therefore, only the first resonant mode can be induced under this operation. The DC voltage frequency response evaluated at the optimal load $R_L = 220$ kΩ is plotted in Fig. 6(a). The analytic predictions obtained from

	M (kg)	η (N·sec/m)	K (N/m)	Θ (N/V)	C_p (nF)	f^{sc} (Hz)
1st	1.23×10^{-3}	5.14×10^{-3}	110.0	1.088×10^{-4}	12.8	47.6
2nd	4.05×10^{-3}	108.24×10^{-3}	10006.0	8.412×10^{-4}	12.8	250.1

Table 3. Equivalent parameters of the device under the two-point rotary magnetic plucking. The notation f^{sc} denotes the short-circuit resonant frequency.

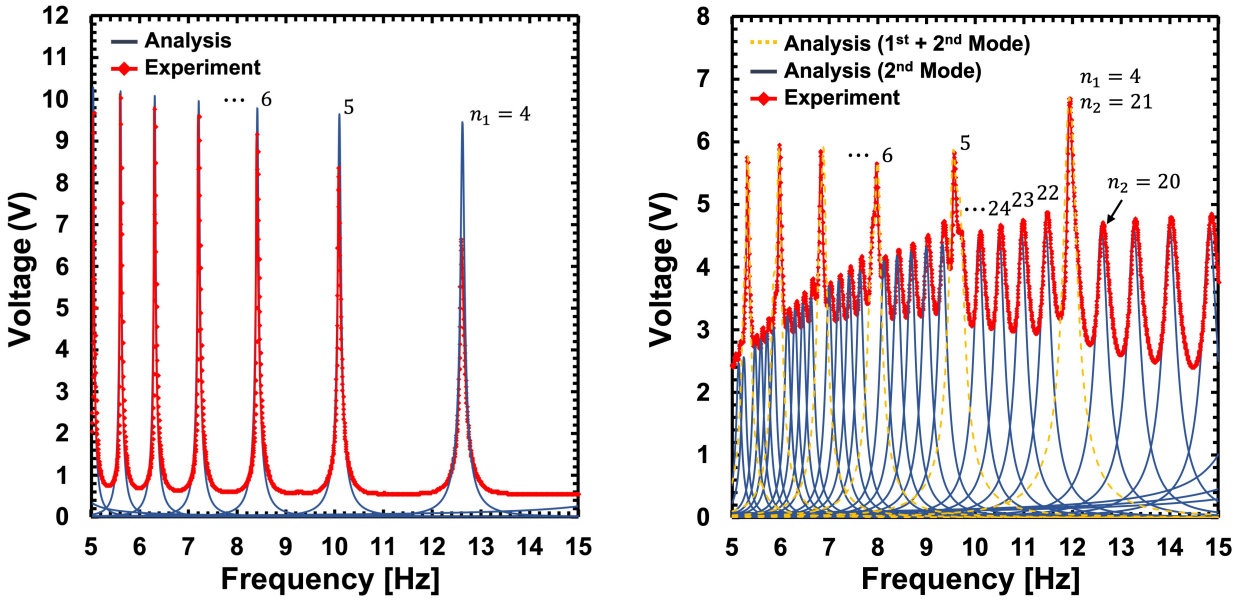

(a) (b)

Figure 6. The comparison of DC voltage response against frequency between the analysis and experiment. (a) is the setup excited by the one-point rotary magnetic plucking. (b) is the setup operated by the two-point rotary magnetic plucking.

Eq. (9) with parameters given by Table 2 are presented individually by various continuous blue curves according to distinct integers $n_1 = 4, \cdots 9$. They are found in reasonable agreement with the experimental observations presented by red points. Notice that the diode loss inevitable in the practical power conditioning process is not taken into account in the previous theoretical modeling. It is included here by setting the voltage drop 1.4 volt in equation (A4) proposed by Wu et al [22] for the fair comparison between the prediction and experiment. The details of description are omitted for brevity. The next observation is that the harvested DC voltage is concentrated on certain specific discrete frequencies of narrow band, such as 5.6 Hz ($n_1 = 9$), 6.3 Hz ($n_1 = 8$), 7.2 Hz ($n_1 = 7$), 8.4 Hz ($n_1 = 6$), 10.0 Hz ($n_1 = 5$) and 12.6 Hz ($n_1 = 4$), etc. However, it is immediately reduced from the peak value of 7-10 volt to 0.6 volt within the adjacent frequencies of peak output described above, as clearly demonstrated in Fig. 6(a). Finally, the time waveform of the piezoelectric voltage measured at around $f_d = 12.6$ Hz ($n_1 = 4$) is shown in Fig. 7(a). Its FFT plot presented in Fig. 7(d) exhibits a sharp peak located at around 50 Hz which is close to f^{sc} of the device (see Table 2) in the frequency

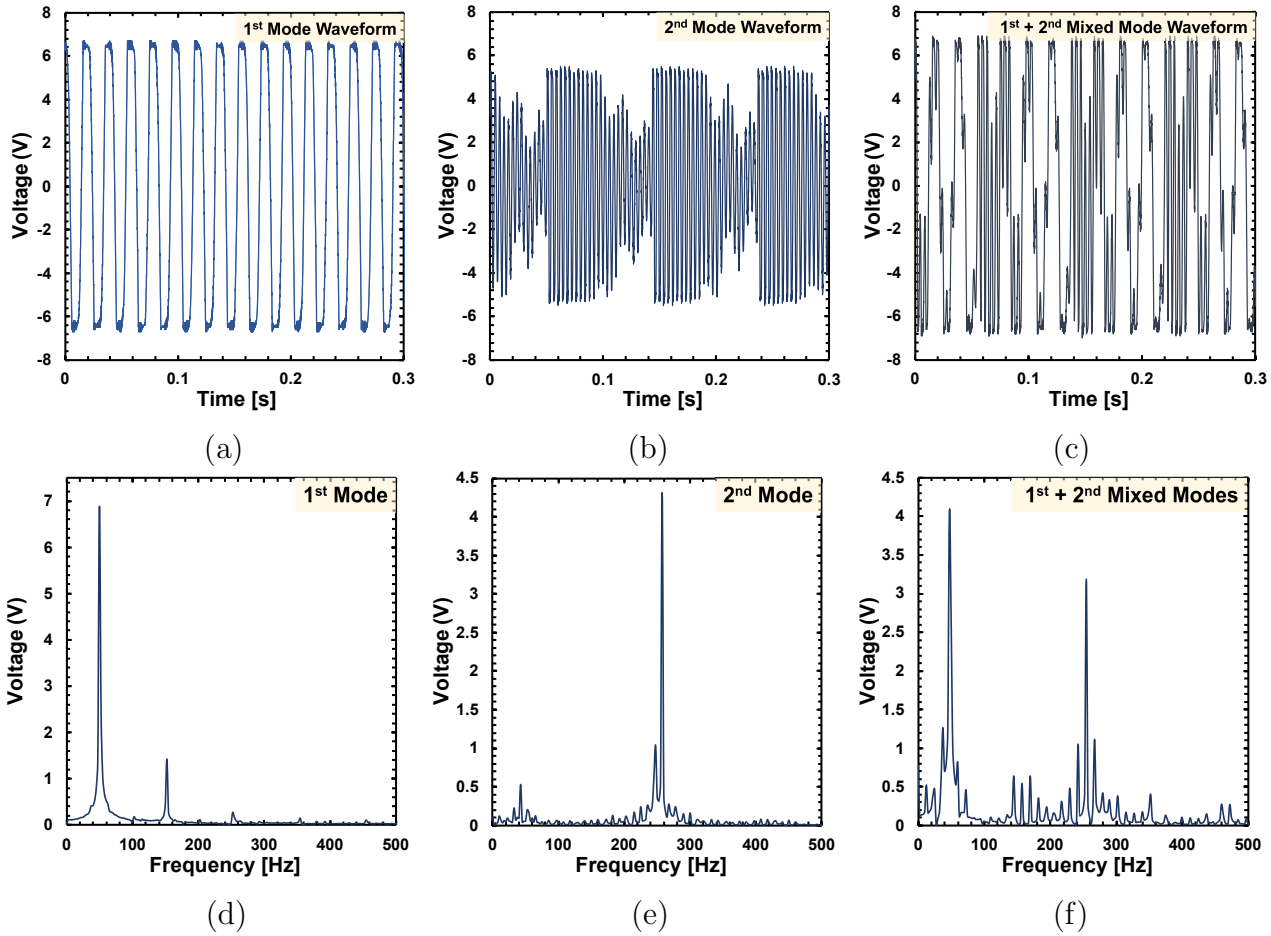

Figure 7. The top three are the time waveforms of the piezoelectric voltage: (a) is measured from the peak voltage of $n_1 = 4$ in Fig. 6(a); (b) is measured from the peak voltage of $n_2 = 24$ (second resonant mode) in Fig. 6(b); (c) is measured from the peak voltage of $n_1 = 4$ and $n_2 = 21$ (mixing of the first two resonant modes) in Fig. 6(b). Next, the bottom three (d), (e) and (f) are the corresponding FFT plots of the cases (a), (b) and (c), respectively.

domain. This confirms the harmonic extracted from the voltage frequency response in Fig. 6(a) is mainly attributed to the first resonant mode of the harvester.

On the other hand, the electrical response of the second setup allowing two-point rotary magnetic plucking exhibits the significant contrast in comparison to the previous case. Indeed, the DC voltage frequency response evaluated at the load $R_L = 220$ kΩ is shown in Fig. 6(b) where the experimental observations are presented by red points. The analytic predictions are obtained from Eq. (25) evaluated at various integers n_1 and n_2. They are presented by blue curves for the second resonant mode of vibration and are presented by yellow curves for the mixed resonant modes of vibration, respectively. Obviously, Fig. 6(b) shows a good agreement with the experimental observations. In addition, the discussions of these results are classified into two cases according to the different types of resonant modes.

(I) Suppose only the second resonant mode is triggered by the specific driving frequency f_d; i.e., $f_d \in \mathcal{A}_2$ but $f_d \notin \mathcal{A}_1$ where $\mathcal{A}_1$ and $\mathcal{A}_2$ are defined by Eq. (1) and Eq. (2). An example of this case is $f_d = 10.4$ Hz and $n_2 = 24$ in Fig. 6(b) so that $n_2 f_d \approx f_2^{\rm sc} = 250.1$ Hz. The waveform of the piezoelectric voltage is shown in Fig. 7(b) and its FFT plot shown in Fig. 7(e) justifies the main contribution of harmonics results from the second resonant mode of vibration. In addition, from Fig. 6(b), the lowest magnitude of measured DC output voltage is about 3.0 volt within the frequency range between 10 to 12 Hz. This range is within the adjacent frequencies of peak voltage labelled by $n_1 = 5$ and $n_1 = 4$, as shown in Fig. 6(b). In comparison with the off-resonant frequency range between 10.5-12 Hz (the neighboring frequency between the peaks labelled by $n_1 = 5$ and $n_1 = 4$) shown in Fig. 6(a), the DC voltage generated by the first setup is as low as around 0.6 volt. It shows that the harvested power is increased up to 2500% ($= (3/0.6)^2 \times 100\%$) in the off-resonance region of Fig. 6(a). This confirms the proposed device offers an advantage of inducing broadband frequency up-conversion operated by two-point rotary magnetic plucking.

(II) Suppose both the first two resonant modes of vibration are induced by some driving frequency f_d; i.e., $f_d \in \mathcal{A}_1$ and $f_d \in \mathcal{A}_2$. In other words, there exist some integers n_1 and n_2 such that the driving frequency f_d satisfies the conditions $n_1 f_d \approx f_1^{\rm sc} = 47.6$ Hz and $n_2 f_d \approx f_2^{\rm sc} = 250.1$ Hz. An example of it is $f_d \approx 11.9$ Hz, $n_1 = 4$ and $n_2 = 21$ as illustrated in Fig. 6(b). The corresponding time waveform of the piezoelectric voltage is shown in Fig. 7(c) and its FFT presentation is shown in Fig. 7(f). Clearly, the FFT plot exhibits two very sharp peaks evaluated at around 47 Hz and 250 Hz. This provides an additional proof showing the harmonics extracted from Fig. 7(c) are mainly attributed to the mixing of the first two resonant vibrations. A consequence of it is that the output voltage is enhanced to 6.7 volt, giving rise to significant power boosting in comparison with the previous case (I).

A closing remark is about the feasibility of using Eq. (26) for replacing the complex formula Eq. (25). Indeed, it can be shown that in the present case the contributions to the total power output from the crossing terms $G_{12} = G_{21}$ in Eq. (23) are less than 0.15%. Thus, the use of Eq. (26) is legitimate as long as the resonant frequencies of the device are widely separated.

5. Conclusions

The article shows the significant broadband energy harvesting that can be accomplished by inducing the mixed resonant modes of vibration under the two-point rotary magnetic plucking. The proposed device consists of a piezoelectric cantilever beam connected to the standard AC-DC interface circuit. It is designed to allow the two impulsive magnetic forces with opposite directions, acting simultaneously on the beam so that the second resonant mode of vibration can be induced by impulsive excitation. A theoretical model is established for explaining the

electrical response of the proposed harvester. It is based on the Fourier decomposition of magnetic impulsive forces and the equivalent load impedance originally proposed for analyzing harvester arrays. The former is for realizing the phenomenon of frequency up-conversion and the latter is for the replacement of nonlinear interface circuit. The analytic estimate of DC power output is derived considering the effect of mixed resonant modes of vibration.

The predictions are validated by experiment carried out under the two different scenarios. The first one adopts the conventional approach allowing the plucking only at the tip magnet (one-point magnetic plucking), giving rise to inducing a single resonant mode of vibration. It exhibits the significant output voltage generated at several discrete number of driving frequencies. However, the voltage drops to 0.6 volt in the off-resonance region between the adjacent frequencies of peak voltage, as shown in Fig. 6(a). Such a drawback is overcome by the proposed setup allowing the two-point magnetic plucking for triggering mixed resonant modes, as confirmed by Fig. 6(b). In addition, the lowest level of output voltage is observed to be around 3 volt within the wide frequency range between 5-15 Hz. Thus, the DC output power is enhanced at least to 2500% higher than that in the off-resonant frequencies of the first setup, showing the remarkable feature of broadband energy harvesting.

Acknowledgments

The support from Ministry of Science and Technology through the grant no 108-2221-E-002-004-MY3 is highly appreciated.

References

[1] A. Erturk and D. J. Inman. *Piezoelectric Energy Harvesting*. Wiley, 2011.

[2] Z. Yang, S. Zhou, J. Zu, and D. Inman. High-Performance Piezoelectric Energy Harvesters and Their Applications. *Joule*, **2**:642–697, 2018.

[3] Y. Liao and H. A. Sodano. Model of a Single Mode Energy Harvester and Properties for Optimal Power Generation. *Smart Materials and Structures*, **17**:065026, 2008.

[4] S. Roundy and P. K. Wright. A Piezoelectric Vibration Based Generator for Wireless Electronics. *Smart Materials and Structures*, **13**:1131–1142, 2004.

[5] Y. C. Shu and I. C. Lien. Analysis of Power Output for Piezoelectric Energy Harvesting Systems. *Smart Materials and Structures*, **15**:1499–1512, 2006.

[6] D. Guyomar, A. Badel, E. Lefeuvre, and C. Richard. Toward Energy Harvesting Using Active Materials and Conversion Improvement by Nonlinear Processing. *IEEE Transaction on Ultrasonics, Ferroelectrics, and Frequency Control*, **52**:584–595, 2005.

[7] Y. C. Shu, I. C. Lien, and W. J. Wu. An Improved Analysis of the SSHI Interface in Piezoelectric Energy Harvesting. *Smart Materials and Structures*, **16**:2253–2264, 2007.

[8] M. Lallart and D. Guyomar. An Optimized Self-Powered Switching Circuit for Non-Linear Energy Harvesting with Low Voltage Output. *Smart Materials and Structures*, **17**:035030, 2008.

[9] E. Lefeuvre, A. Badel, C. Richard, and D. Guyomar. Piezoelectric Energy Harvesting Device Optimization by Synchronous Electric Charge Extraction. *Journal of Intelligent Material Systems and Structures*, **16**:865–876, 2005.

[10] L. Tang and Y. Yang. Analysis of Synchronized Charge Extraction for Piezoelectric Energy Harvesting. *Smart Materials and Structures*, **20**:085022, 2011.

[11] M. F. Lumentut and Y. C. Shu. Shunted Optimal Vibration Energy Harvesting Control of Discontinuous Smart Beams. *Composite Structures*, **242**:112126, 2020.

[12] A. Keshmiri, N. Wu, and Q. Wang. A New Nonlinearly Tapered FGM Piezoelectric Energy Harvester. *Engineering Structures*, **173**:52–60, 2018.

[13] J. Xu and J. Tang. Modeling and Analysis of Piezoelectric Cantilever-Pendulum System for Multi-Directional Energy Harvesting. *Journal of Intelligent Material Systems and Structures*, **28**:323–338, 2017.

[14] W. Zhou, B. Wang, C. W. Lim, and Z. Yang. A Distributed-Parameter Electromechanical Coupling Model for a Segmented Arc-Shaped Piezoelectric Energy Harvester. *Mechanical Systems and Signal Processing*, **146**:107005, 2021.

[15] M. F. Lumentut and Y. C. Shu. A Unified Electromechanical Finite Element Dynamic Analysis of Multiple Segmented Smart Plate Energy Harvesters: Circuit Connection Patterns. *Acta Mechanica*, **229**:4575–4604, 2018.

[16] M. F. Lumentut and Y. C. Shu. Network Segmentations of Smart Plate Structure with Attached Mass and Dynamic Motions. *European Journal of Mechanics / A Solids*, **85**:104061, 2021.

[17] B. Bayik, A. Aghakhani, I. Basdogan, and A. Erturk. Equivalent Circuit Modeling of a Piezo-Patch Energy Harvester on a Thin Plate with AC-DC Conversion. *Smart Structures and Systems*, **25**:055015, 2016.

[18] I. C. Lien and Y. C. Shu. Array of Piezoelectric Energy Harvesting by Equivalent Impedance Approach. *Smart Materials and Structures*, **21**:082001, 2012.

[19] H. C. Lin, P. H. Wu, I. C. Lien, and Y. C. Shu. Analysis of an Array of Piezoelectric Energy Harvesters Connected in Series. *Smart Materials and Structures*, **22**:094026, 2013.

[20] P. H. Wu and Y. C. Shu. Finite Element Modeling of Electrically Rectified Piezoelectric Energy Harvesters. *Smart Materials and Structures*, **24**:094008, 2015.

[21] P. H. Wu, Y. J. Chen, B. Y. Li, and Y. C. Shu. Wideband Energy Harvesting Based on Mixed Connection of Piezoelectric Oscillators. *Smart Materials and Structures*, **26**:094005, 2017.

[22] P. H. Wu, J. T. Lin, Y. C. Lo, and Y. C. Shu. An SECE Array of Piezoelectric Energy Harvesting. *Smart Materials and Structures*, **30**:045008, 2021.

[23] Y. Zhang, K. Bian, Y. Gu, M. Ye, W. Tian, and W. Liu. Cost-Effective and Scalable Rectifier Design for Multiple Piezoelectric Power Sources with Improved Performance. *Journal of Intelligent Material Systems and Structures*, **31**:167–181, 2020.

[24] X. Wang, Y. Xia, Y. Du, H. Xia, G. Shi, Y. Ye, and Z. Chen. Multi-Input SECE Based on Buck Structure for Piezoelectric Energy Harvesting. *IEEE Tranactions on Power Electronics*, **36**:3638–3642, 2021.

[25] S. Roundy, E. S. Leland, J. Baker, E. Carleton, E. Reilly, E. Lai, B. Otis, J. M. Rabaey, P. K. Wright, and V. Sundararajan. Improving Power Output for Vibration-Based Energy Scavengers. *IEEE Pervasive Computing*, **4**:28–36, 2005.

[26] A. Erturk, J. M. Renno, and D. J. Inman. Modeling of Piezoelectric Energy Harvesting from an L-Shaped Beam-mass Structure with an Application to UAVs. *Journal of Intelligent Material Systems and Structures*, **20**:529–544, 2009.

[27] D. F. Berdy, B. Jung, J. F. Rhoads, and D. Peroulis. Wide-Bandwidth, Meandering Vibration Energy Harvester with Distributed Circuit Board Inertial Mass. *Sensors and Actuators A: Physical*, **188**:148–157, 2012.

[28] M. Rezaeisaray, M. E. Gowini, D. Sameoto, D. Raboud, and W. Moussa. Low Frequency Piezoelectric Energy Harvesting at Multi Vibration Mode Shapes. *Sensors and Actuators A: Physical*, **228**:104–111, 2015.

[29] X. Li, D. Upadrashta, K. Yu, and Y. Yang. Analytical Modeling and Validation of Multi-Mode Piezoelectric Energy Harvester. *Mechanical Systems and Signal Processing*, **124**:613–631, 2019.

[30] S. Sun and P. W. Tse. Design and Performance of a Multimodal Vibration-Based Energy Harvester. *Applied Physics Letters*, **110**:243902, 2017.

[31] D. Upadrashta and Y. Yang. Trident-Shaped Multimodal Piezoelectric Energy Harvester. *Journal of Aerospace Engineering*, **31**:04018070, 2018.

[32] H. Xiao, X. Wang, and S. John. A Multi-Degree of Freedom Piezoelectric Vibration Energy Harvester with Piezoelectric Elements Inserted between Two Nearby Oscillators. *Mechanical Systems and Signal Processing*, **68-69**:138–154, 2016.

[33] C. Duan, J. Peng, J. Song, Q. Bai, J. Peng, J. Tao, and X. Zheng. Multi-Factors Analysis on the Energy Harvesting Performance of PEH under Multiple-Frequency Excitation. *Smart Materials and Structures*, **29**:085025, 2020.

[34] I. H. Kim, H. J. Jung, B. M. Lee, and S. J. Jang. Broadband Energy-Harvesting Using a Two Degree-of-Freedom Vibrating Body. *Applied Physics Letters*, **98**:214102, 2011.

[35] W. Zhou, G. R. Penamalli, and L. Zuo. An Efficient Vibration Energy Harvester with a Multi-Mode Dynamic Magnifier. *Smart Materials and Structures*, **21**:015014, 2012.

[36] M. M. Ahmad, N. M. Khan, and F. U. Khan. Review of Frequency Up-Conversion Vibration Energy Harvesters Using Impact and Plucking Mechanism. *International Journal of Energy Research*, 2021. https://doi.org/10.1002/er.6832.

[37] T. Xue, H. G. Yeo, S. Trolier-McKinstry, and S. Roundy. Wearable Inertial Energy Harvester with Sputtered Bimorph Lead Zirconate Titanate (PZT) Thin-Film Beams. *Smart Materials and Structures*, **27**:085026, 2018.

[38] R. Dauksevicius, R. Gaidys, V. Ostasevicius, R. Lockhart, A. V. Quintero, N. de Rooij, and D. Briand. Nonlinear Piezoelectric Vibration Energy Harvester with Frequency-Tuned Impacting Resonators for Improving Broadband Performance at Low Frequencies. *Smart Materials and Structures*, **28**:025025, 2019.

[39] M. Pozzi. Impulse Excitation of Piezoelectric Bimorphs for Energy Harvesting: a Dimensionless Model. *Smart Materials and Structures*, **23**:045044, 2014.

[40] X. Rui, Y. Zhang, Z. Zeng, G. Yue, X. Huang, and J. Li. Design and Analysis of a Broadband Three-Beam Impact Piezoelectric Energy Harvester for Low-Frequency Rotational Motion. *Mechanical Systems and Signal Processing*, **149**:107307, 2021.

[41] B Kathpalia, D. Tan, I. Stern, and A. Erturk. An Experimentally Validated Model for Geometrically Nonlinear Plucking-Based Frequency Up-Conversion in Energy Harvesting. *Smart Materials and Structures*, **27**:015024, 2018.

[42] P. Pillatsch, E. M. Yeatman, and A. S. Holmes. Magnetic Plucking of Piezoelectric Beams for Frequency Up Converting Energy Harvesters. *Smart Materials and Structures*, **23**:025009, 2014.

[43] Y. Kuang, Z. Yang, and M. Zhu. Design and Characterisation of a Piezoelectric Knee-Joint Energy Harvester with Frequency Up-Conversion Through Magnetic Plucking. *Smart Materials and Structures*, **25**:085029, 2016.

[44] P. Panthongsy, D. Isarakorn, P. Janphuang, and K. Hamamoto. Fabrication and Evaluation of Energy Harvesting Floor Using Piezoelectric Frequency Up-Converting Mechanism. *Sensors and Actuators A*, **279**:321–330, 2018.

[45] F. Wang, A. Abedini, T. Alghamdi, and S. Onsorynezhad. Bimodal Approach of a Frequency-Up-Conversion Piezoelectric Energy Harvester. *International Journal of Structural Stability and Dynamics*, **19**:1950090, 2019.

[46] L. Zhao and Y. Yang. An Impact-Based Broadband Aeroelastic Energy Harvester for Concurrent Wind and Base Vibration Energy Harvesting. *Applied Energy*, **212**:233–243, 2018.

[47] M. Pozzi. Plucked Piezoelectric Bimorphs for Knee-Joint Energy Harvesting: Modelling and Experimental Validation. *Smart Materials and Structures*, **20**:055007, 2011.

[48] X. Fu and W. H. Liao. Modeling and Analysis of Piezoelectric Energy Harvesting with Dynamic Plucking Mechanism. *ASME Journal of Vibration and Acoustics*, **141**:031002, 2019.

[49] S. Fang, X. Fu, and W. H. Liao. Asymmetric Plucking Bistable Energy Harvester: Modeling and Experimental Validation. *Journal of Sound and Vibration*, **459**:114852, 2019.

[50] S. Fang, X. Fu, and W. H. Liao. Modeling and Experimental Validation on the Interference of Mechanical

Plucking Energy Harvesting. *Mechanical Systems and Signal Processing*, **134**:106317, 2019.

[51] Y. C. Shu, W. C. Wang, and Y. P. Chang. Electrically Rectified Piezoelectric Energy Harvesting Induced by Rotary Magnetic Plucking. *Smart Materials and Structures*, **27**:125006, 2018.

[52] H. Fu and E. M. Yeatman. Rotational Energy Harvesting Using Bi-Stability and Frequency Up-Conversion for Low-Power Sensing Applications: Theoretical Modelling and Experimental Validation. *Mechanical Systems and Signal Processing*, **125**:229–244, 2019.

[53] R. Dauksevicius, A. Kleiva, and V. Grigaliunas. Analysis of Magnetic Plucking Dynamics in a Frequency Up-Converting Piezoelectric Energy Harvester. *Smart Materials and Structures*, **27**:085016, 2018.

[54] Z. Xie, C. A. Kitio Kwuimy, Z. Wang, and W. Huang. A Piezoelectric Energy Harvester for Broadband Rotational Excitation Using Buckled Beam. *AIP Advances*, **8**:015125, 2018.

[55] A. M. Wickenheiser and E. Garcia. Broadband Vibration-Based Energy Harvesting Improvement through Frequency Up-Conversion by Magnetic Excitation. *Smart Materials and Structures*, **19**:065020, 2010.

[56] M. Cai, J. Wang, and W. H. Liao. Self-Powered Smart Watch and Wristband Enabled by Embedded Generator. *Applied Energy*, **263**:114682, 2020.

[57] M. Cai and W. H. Liao. Design, Modeling and Experiments of Electromagnetic Energy Harvester Embedded in Smart Watch and Wristband as Power Source. *IEEE/ASME Transactions on Mechatronics*, 2021. DOI: 10.1109/TMECH.2020.3032536.

[58] H. G. Yeo, T. Xue, S. Roundy, X. Ma, C. Rahn, and S. Trolier-McKinstry. Strongly (001) Oriented Bimorph PZT Film on Metal Foils Grown by *rf*-Sputtering for Wrist-Worn Piezoelectric Energy Harvesters. *Advanced Functional Materials*, **28**:1801327, 2018.

[59] P. Pillatsch, E. M. Yeatman, and A. S. Holmes. A Piezoelectric Frequency Up-Converting Energy Harvester with Rotating Proof Mass for Human Body Applications. *Sensors and Actuators A: Physical*, **206**:178–185, 2014.

[60] Y. H. Fu. Micro Piezoelectric Energy Harvester Applied in Broadband Rotational Energy Harvesting System. MS. Thesis. *National Taiwan Univesity*, 2018.

[61] H. Fu and E. M. Yeatman. A Methodology for Low-Speed Broadband Rotational Energy Harvesting Using Piezoelectric Transduction and Frequency Up-Conversion. *Energy*, **125**:152–161, 2017.

[62] T. Xue and S. Roundy. On Magnetic Plucking Configurations for Frequency Up-Converting mechanical Energy Harvesters. *Sensors and Actuators A*, **253**:101–111, 2017.

[63] R. Ramezanpour, H. Nahvi, and S. Ziaei-Rad. A Vibration-Based Energy Harvester Suitable for Low-Frequency, High-Amplitude Environments: Theoretical and Experimental Investigations. *Journal of Intelligent Material Systems and Structures*, **27**:642–665, 2016.

[64] W. H. Wu, K. C. Kuo, Y. H. Lin, and Y. C. Tsai. Non-Contact Magnetic Cantilever-Type Piezoelectric Energy Harvester for Rotational Mechanism. *Microelectronic Engineering*, **191**:16–19, 2018.

[65] A. Abdelkefi, N. Barsallo, L. Tang, Y. Yang, and M. R. Hajj. Modeling, Validation, and Performance of Low-Frequency Piezoelectric Energy Harvesters. *Journal of Intelligent Material Systems and Structures*, **25**:1429–1444, 2014.

[66] G. Hu, L. Tang, J. Liang, and R. Das. Modelling of a Cantilevered Energy Harvester with Partial Piezoelectric Coverage and Shunted to Practical Interface Circuits. *Journal of Intelligent Material Systems and Structures*, **30**:1896–1912, 2019.